THE CONCEPT OF HIGH-LIFT, MILD STALL WING

Alexander Nagel and Misha Shepshelovich

Engineering Center, Israel Aircraft Industries

Keywords: *airfoils, wings, high lift, UAV , mild stall;*

Abstract

High-lift, mild stall wings are attractive for development of small and medium size UAV. This is especially true for evaluation of configurations with increased level of parasite drag, where optimum endurance performance is realized at high loitering lift coefficients, leading to a very demanding requirements for maximum lift. High-lift, mild-stall wings allow relaxation of imposed speed safety margin and extension of allowable range of flight lift coefficients. This helps to recover endurance performance, provide a safe flight in ghusty air and improve aircraft response to symmetric and asymmetric stall. For mild stall wings, the speed limitation imposed on take-off and landing may be reconsidered, improving the ground performance of UAV and promoting further the issue of automatic take-off and landing. The performed conceptual evaluation of high-lift, mild stall airfoils prepares the ground for development of the wings adjusted to specific requirements of operational UAV.

Nomenclature

C_l	-	airfoil lift coefficient
C_d	-	airfoil drag coefficient
C_p	-	pressure coefficient
C_m	-	airfoil pitching moment
C_L	-	aircraft lift coefficient
C_D	-	aircraft drag coefficient
$C_{l\,max}$	-	airfoil maximum lift
$C_{D\,0}$	-	aircraft zero lift drag
$C_L^{1.5}/C_D$	-	aircraft endurance factor
Re	-	chord Reynolds number
x/c	-	chord fraction
t/c	-	thickness ratio
e	-	spanload efficiency
α	-	angle of attack
δ_{ail}	-	aileron deflection angle
WT	-	wind tunnel
MS	-	Mild Stall
AR	-	aspect ratio
UAV	-	Unmanned Air Vehicle
IAI	-	Israel Aircraft Industries

1. Introduction

High-lift wings are benifitial for endurance performance of UAV with increased parasite drag. (refs. 1-4). This is especially evident in development of configurations with high aspect ratio wings, where optimum endurance performance tends to deviate to high loitering lift coefficients with increase of parasite drag (Fig.1). This results in very demanding requirements for maximum lift, that were answered in development of IAI long endurance UAV by design of two-element, high-lift airfoils.

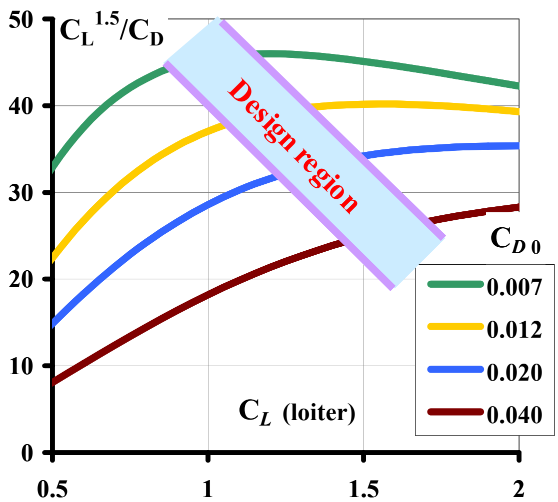

Fig. 1. Design region of UAV with high aspect ratio wings, AR= 25, e= 0.85.

The situation is similar for small and medium size UAV with their moderate aspect ratio wings (Fig. 2). For these cases, engine-airframe integration, drag-consuming payload installations, non-retractable landing gear, etc. contribute to aircraft parasite drag, increasing attractivity of high-lift wings.

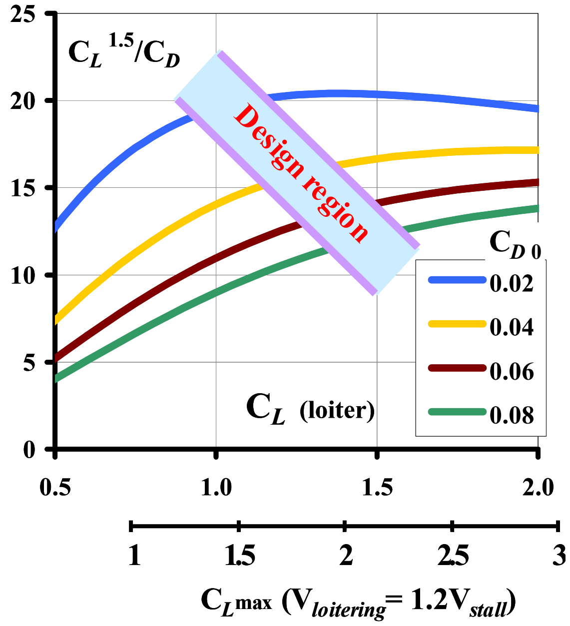

Fig. 2. Design region of UAV with moderate aspect ratio wings, AR= 12, e= 0.85.

Mild stall characteristics produce a further advantages in development of UAV configurations. The following benefits were identified for this case:

- Mild stall wings are benifitial for flight safety of small and medium size UAV flying at reduced airspeeds in ghusty air. At stall lift coefficients, no significant rolling moments are expected for this type of the wings, improving aircraft response to asymmetric stall and preventing the drop of the wing.
- For conventional wing-tail configuration, mild stall wings produce benifitial nose-down moments close to stalling speeds. This is a result of gradual loss of wing downwash on the tail, leading to a feature of “passive self-recovery at stall in the pitch plane”.
- Required speed safety margin may be revised for mild stall wings, allowing loitering at higher lift coefficients and improving endurance performance of configurations with increased parasite drag.
- Relaxation of speed safety margin helps to improve take-off and landing performance of UAV. This is especially relevant for automatic take-off and landing, where development of flight control may benefit from variation of allowable margins.
- Mild stall wings show reduced sensitivity to contamination effects, providing the possibility to continue a safe flight in unfavorable weather conditions.

Typical cases of abrupt and mild stall of high-lift airfoils were outlined schematically by McMasters and Henderson, showing characteristics of airfoils with concave and highly cambered upper surface (Fig. 3, ref. 5). While high-lift, front-loaded airfoils have a tendency for abrupt stall (ref. 6), the known mild-stall airfoils (refs. 7-9) realize only moderate values of maximum lift. This is illustrated in Figs. 4-5, showing geometry and experimental lift curves of two well-known mild stall airfoils – NACA-4415 and FX61-184.

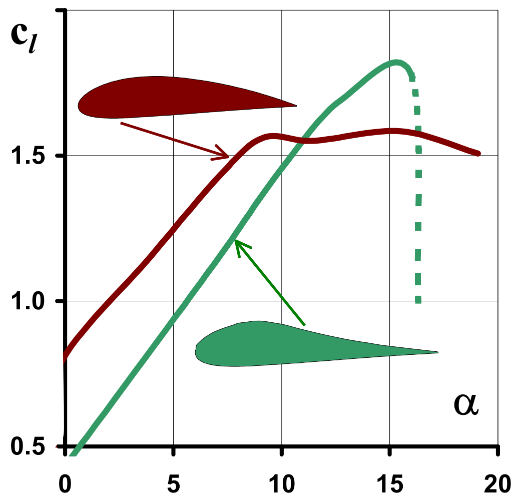

Fig. 3. Abrupt and mild stall patterns (ref. 5)

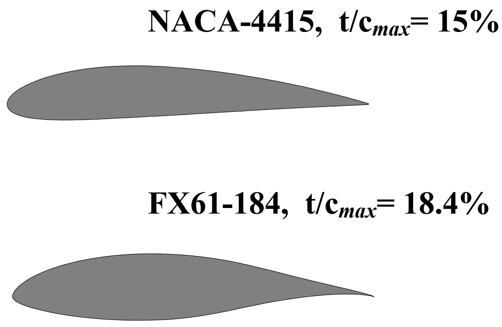

Fig. 4. Mild stall airfoils.

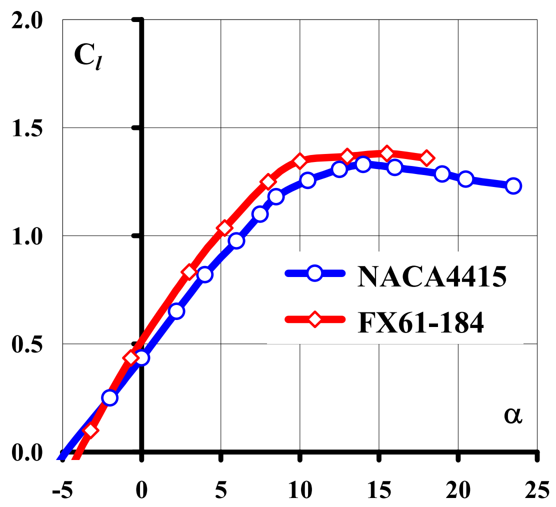

Fig. 5. Lift curves of mild stall airfoils, WT test, Re= $1.0*10^6$.

Maximum lift of subsonic airfoils may be improved by delaying formation of sharp suction peak at their leading edge. This may be achieved by reshaping the forward portion of the airfoil (blunt, or drooped leading edge) as was demonstrated by evaluation of modified NACA and NASA airfoils (refs. 10-11). However, improved maximum lift of these airfoils comes with the tendency for abrupt stall.

The concept of high-lift, mild-stall airfoils relies on combination of blunt leading edge and highly cambered aft portion of the airfoil. The rounded pressure distributing at the forward portion of the airfoil and slowly-creeping trailing edge separation at its aft portion produce the feature of high-lift, mild stall. The first IAI attempt to design an airfoil that is based on these principles was presented in Ref. 1, describing development of airfoil PR8-40. Encouraging results of this evaluation and adoption of MSES code (refs. 12-13) as a main design/analysis tool for airfoils development, justified continuation efforts on design of mild stall airfoils (MS-airfoils).

2. Airfoil PR8-40

Airfoil PR8-40 was designed using inviscid pressure distributions and implementing design principles of high lift mild stall airfoils. Adoption of MSES code for airfoil development allowed theoretical evaluation of this airfoil that was performed after experimental validation.

Geometry of airfoil PR8-40, its lift characteristics and pressure distributions are shown in Figs. 6-10 relative to high-lift airfoil PR7A (ref. 14), illustrating the principal difference in stall pattern of these two airfoils. Continuous lift build-up at the leading edge of airfoil PR8-40 and gradual progress of trailing edge separation at its aft portion produced the desirable mild stall characteristics at high level of lift.

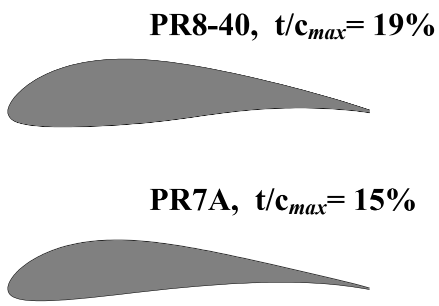

Fig 6. Airfoils PR8-40 and PR7A

Comparison of experimental results with MSES calculations (figs. 11-14) produced valuable information on reliability of MSES code for estimation of airfoils characteristics at stall angles of attack for this particular problem. The confidence in theoretical results allowed a continuation effort on development of MS-airfoils, with a further concentration on design principles supporting the concept of mild stall at high lift coefficients.

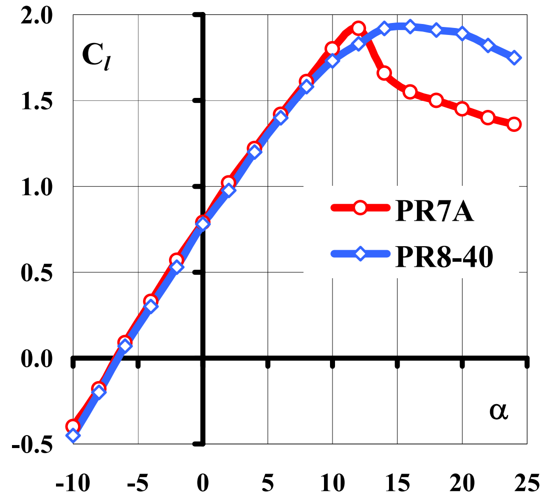

Fig 7. Stall pattern of IAI high-lift airfoils, WT test, Re= $1.0*10^6$.

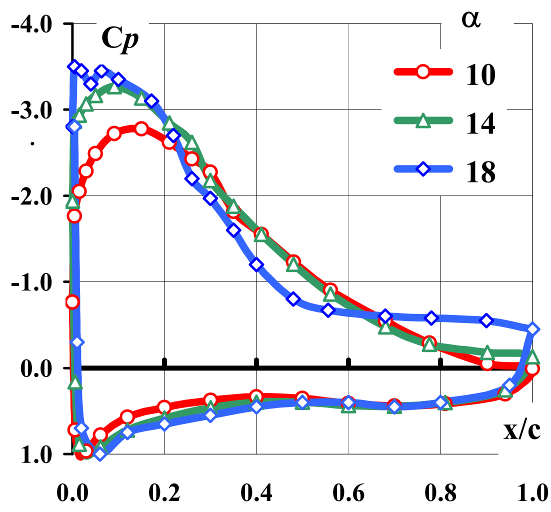

Fig. 10. Airfoil PR8-40 – development of trailing edge separation, WT test, Re= $1.0*10^6$.

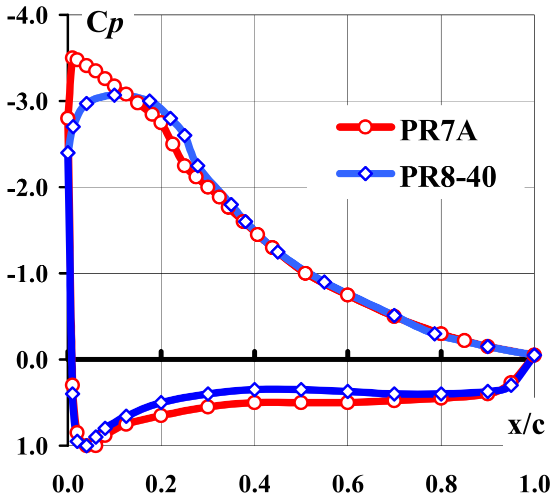

Fig. 8. Comparison of pressure distributions, WT test, Re=$1.0*10^6$, α= 12^0.

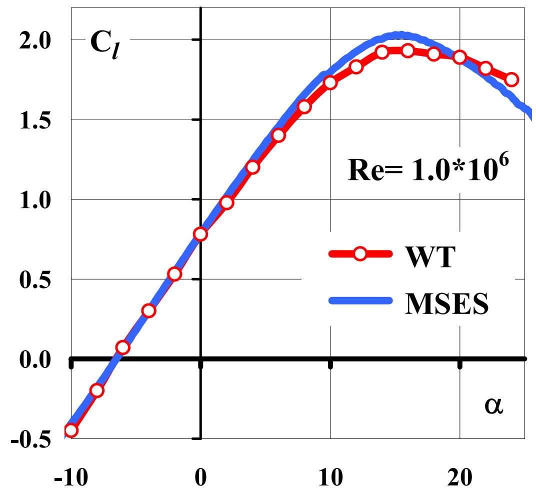

Fig. 11. Airfoil PR8-40 - lift curves, test-theory comparison.

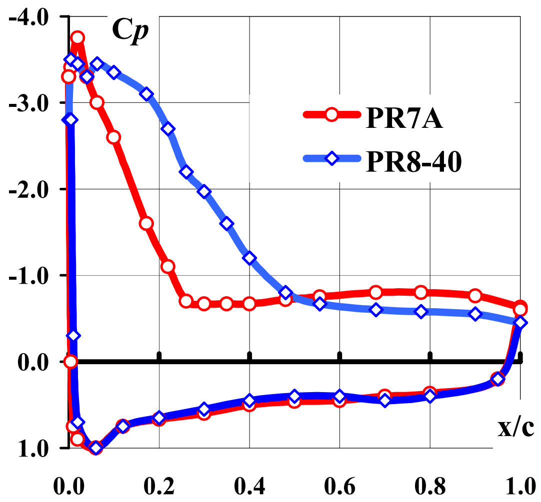

Fig. 9. Comparison of pressure distributions, WT test, Re=$1.0*10^6$, α= 18^0.

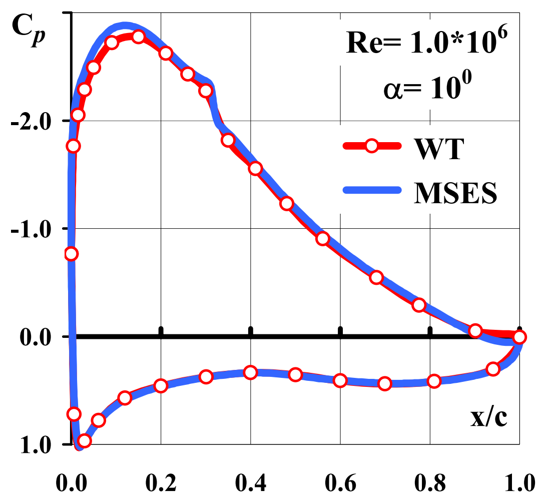

Fig. 12. Airfoil PR8-40 - pressure distributions, test-theory comparison.

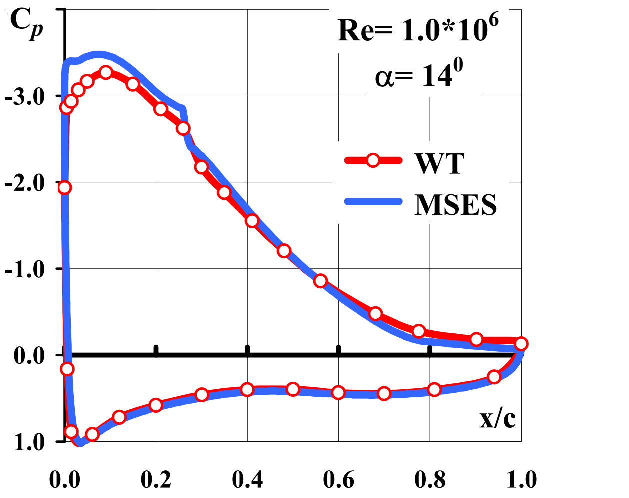

Fig. 13. Airfoil PR8-40 - pressure distributions, test-theory comparison.

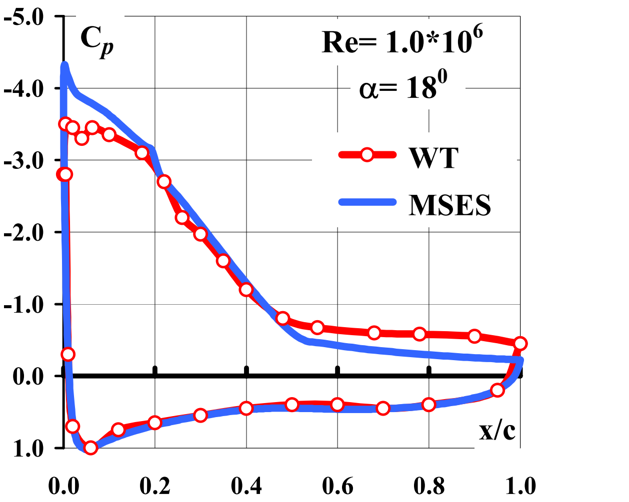

Fig. 14. Airfoil PR8-40 - pressure distributions, test-theory comparison.

3. Development of MS-airfoils

Design goal formulated for continuation effort on development of high-lift, mild-stall airfoils (MS-airfoils, ref. 15) was a further improvement of their stall characteristics. This was achieved by increasing the bluntness of airfoil`s leading edge and by reshaping of their upper surface. Geometry of MS-airfoils and their calculated lift curves are shown in Figs. 15-16, illustrating improvement of stall characteristics relative to the reference case – airfoil PR8-40. The design work was performed at Re=$0.5*10^6$, relying on MSES code.

Improvement of stall characteristics of MS-airfoils (MS-18A and MS-15C) was attributed to slow development of trailing edge separation and to rounded pressure distribution at its forward portion that prevented formation of suction peak at high angles of attack. This is illustrated in Figs. 17-20, showing development of pressure distributions for airfoil MS-18A with increasing angle of attack and by comparing them with pressure distributions of airfoil PR8-40. Comparison of lift and drag characteristics of airfoil MS-15C with NACA-4415 is presented in Figs. 21-22, showing the achieved mild stall at high lift coefficients and drag penalties due to blunt leading edge.

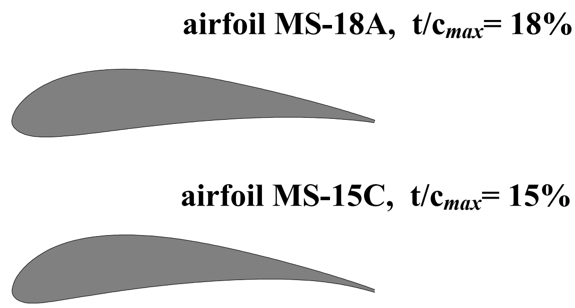

Fig. 15. High-lift, mild stall MS-airfoils.

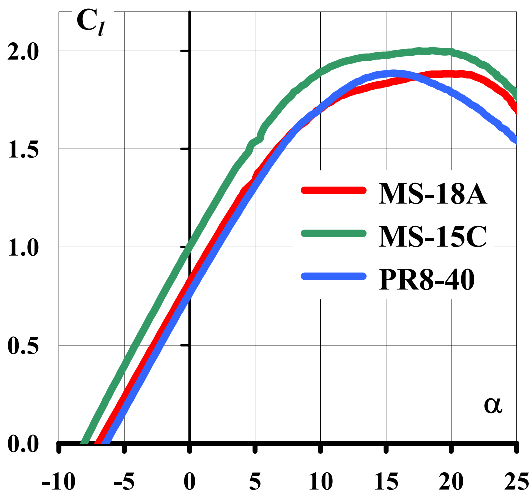

Fig. 16. Lift curves of MS-airfoils, MSES code, Re= $0.5*10^6$.

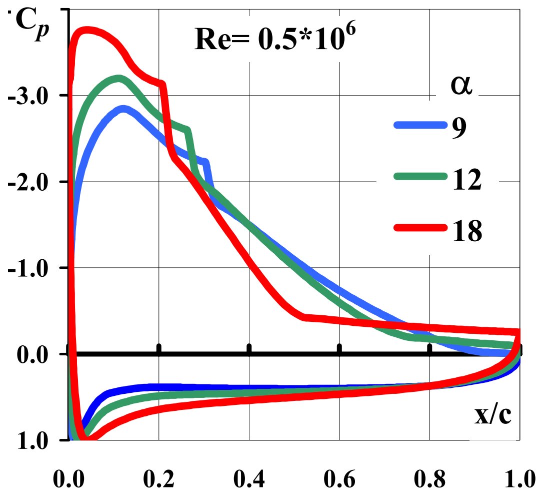

Fig. 17. Airfoil MS-18A – development of trailing edge separation.

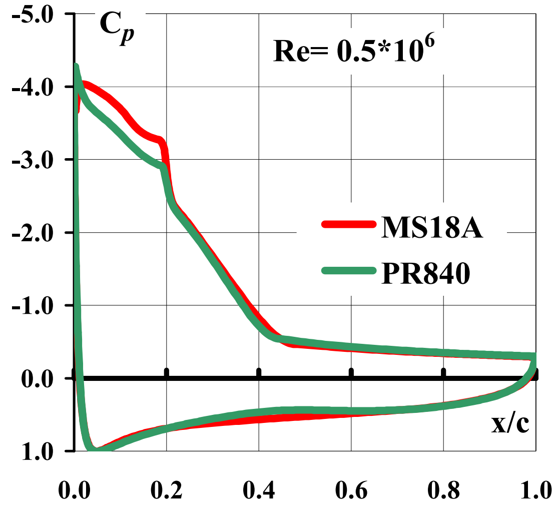

Fig. 20. Comparison of pressure distributions, airfoil MS-18A vs PR8-40, $\alpha= 20^0$.

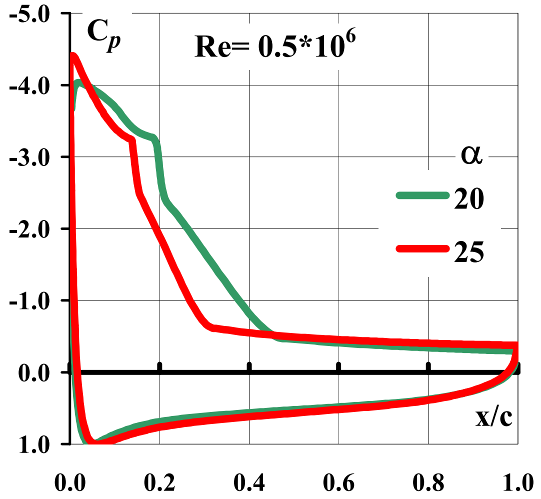

Fig. 18. Airfoil MS-18A – development of trailing edge separation.

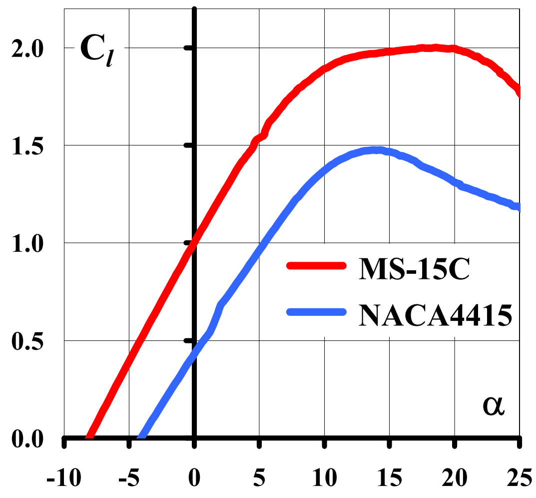

Fig. 21.Airfoil MS-15C vs NACA-4415, lift curves, MSES code, $Re= 0.5*10^6$.

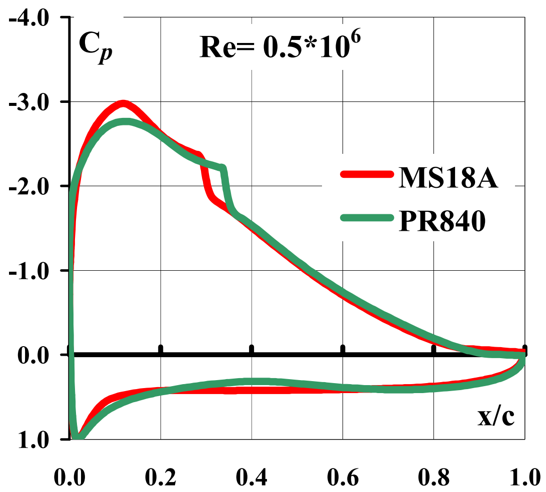

Fig. 19. Comparison of pressure distributions, airfoil MS-18A vs PR8-40, $\alpha= 10^0$.

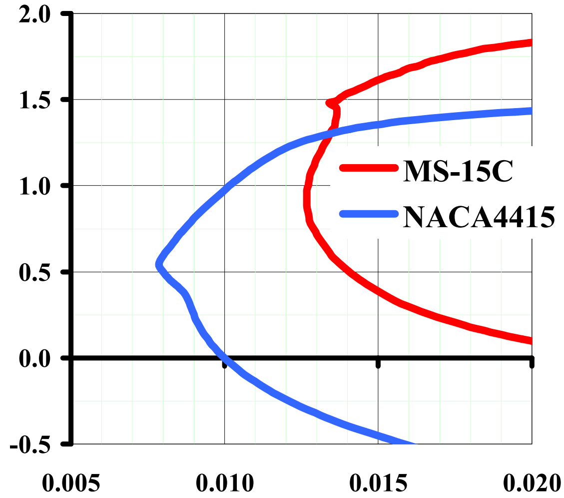

Fig. 22. Airfoil MS-15C vs NACA-4415, drag polars, MSES code, $Re= 0.5*10^6$.

With increasing Reynolds number, the trailing edge separation of MS-airfoils is delayed to higher angles of attack (Figs. 23-24), with a gradual loss of mild stall characteristics above $Re=1.0*10^6$. The best range of Reynolds numbers for MS-airfoils is $Re= 0.5\text{-}1.0*10^6$ – domain of small and medium size UAV.

Contaminated MS-airfoils retain their mild stall characteristics (Figs. 25-27). The loss of maximum lift for this case should be accounted for by limiting the range of loitering lift coefficients with resulting loss of endurance performance.

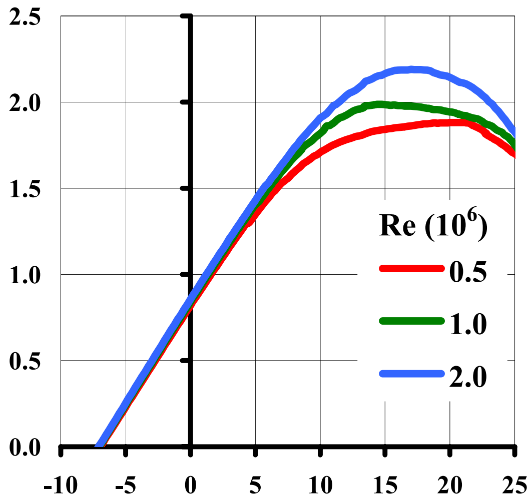

Fig. 23. Airfoil MS-18A - Reynolds effect, lift curves, MSES code.

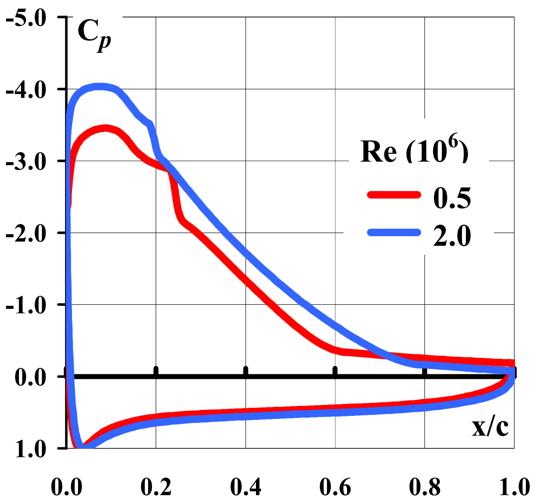

Fig. 24. Airfoil MS-18A – Reynolds effect, pressure distributions, $\alpha= 15^0$.

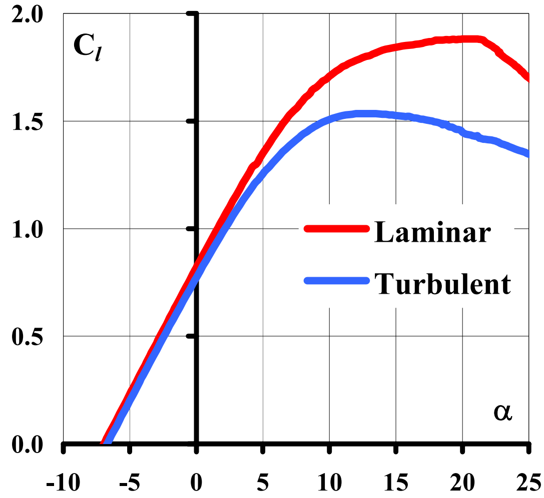

Fig. 25. Airfoil MS-18A - contamination effect, lift curves, $Re= 0.5*10^6$.

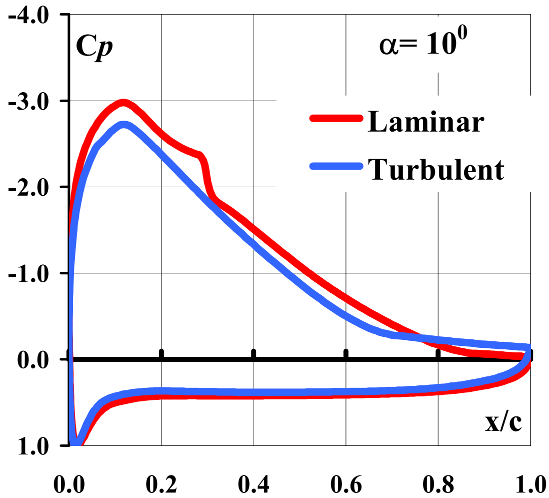

Fig. 26. Airfoil MS-18A - contamination effect, pressure distributions, MSES , $Re= 0.5*10^6$.

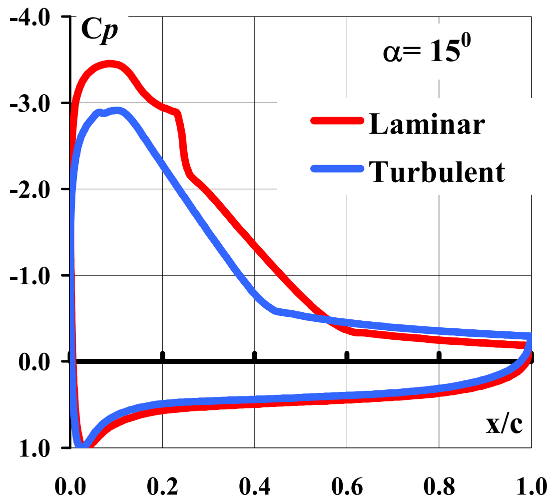

Fig. 27. Airfoil MS-18A - contamination effect, pressure distributions, MSES , $Re= 0.5*10^6$.

Aft-loaded airfoils are difficult for aileron-actuators integration because of their negative hinge moments. This is especially true for the flight at maximum speed, where holding hinge moments of aft-cambered airfoils may put a limitation on available range of the speed. The following rationale was adopted for MS-airfoils on issue of wing-aileron-actuators integration:

- For typical spanload of moderate aspect ratio wings, the outboard location of ailerons makes it possible to modify sectional geometry of aileron stations, aiming for reduction of hinge moments (Fig. 28).
- The simplest possible modification of aft portion of MS-airfoils is definition of aileron`s upper/lower surfaces by straight lines (Fig. 29). This, together with aileron balancing, retain an acceptable aileron effectiveness and produce reduced hinge moments that are more reasonable for aileron-actuators integration (Figs. 30-33)
- A further possible modifications may include reflex camber shape of the aft portion of the aileron, or, slotted aileron with a hinge point located outside the airfoil`s contour for improved aileron effectiveness and control of hinge moments.

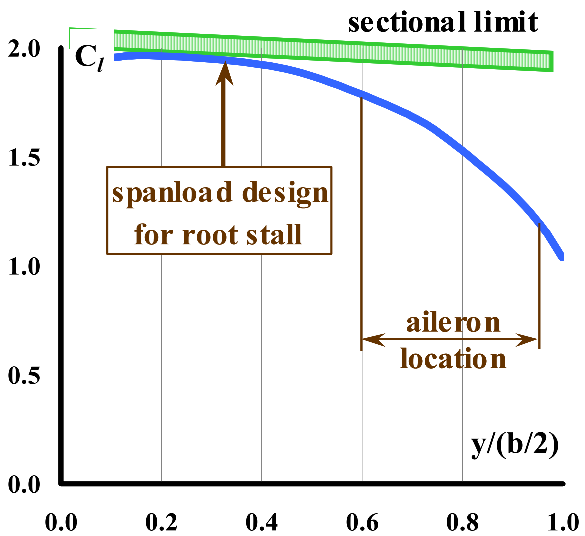

Fig. 28. Typical spanload distribution of moderate aspect ratio wing.

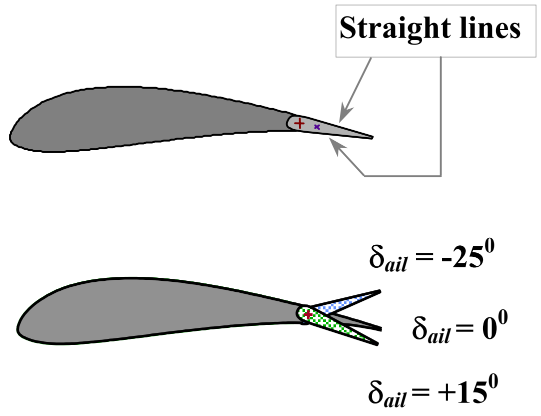

Fig. 29. Airfoil MS-18T – aileron definition.

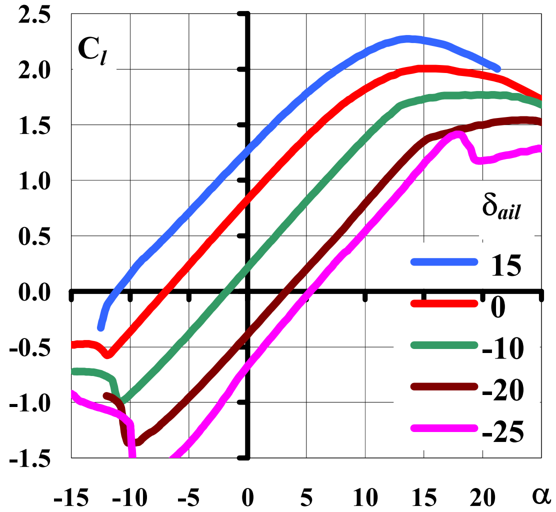

Fig. 30. Airfoil MS-18T - aileron deflections, MSES code, Re= $1.0*10^6$.

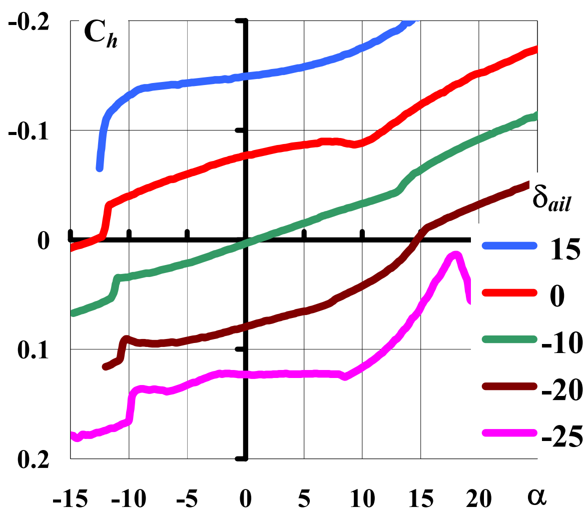

Fig. 31. Airfoil MS-18T - hinge moments, MSES code, Re= $1.0*10^6$.

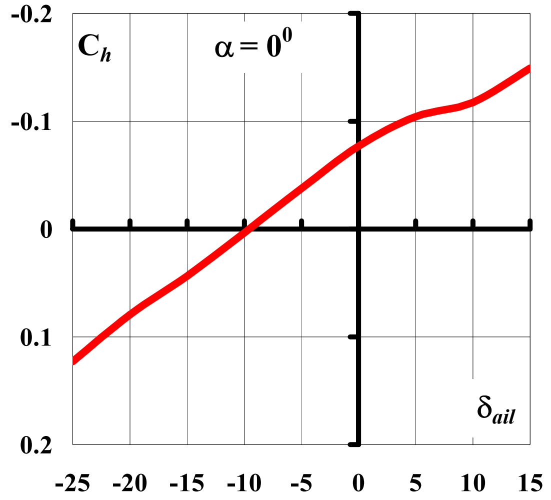

Fig. 32. Aileron hinge moments, Re= $1.0*10^6$.

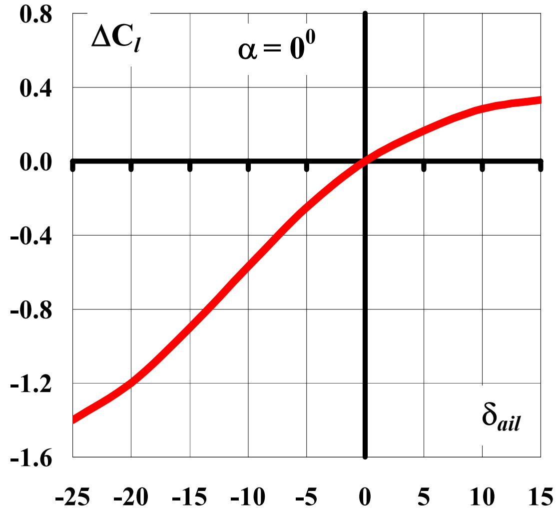

Fig. 33. Aileron effectiveness, Re= $1.0*10^6$.

Conclusions

- The concept of high-lift, mild stall wing relies on "blunt" leading and highly cambered aft portion of the airfoil. The combination of continuous lift build-up at forward portion of MS-airfoils and slowly creeping trailing edge separation with increasing angles of attack produce the feature of mild stall at high lift coefficients.
- The best range of Reynolds numbers for MS-airfoils is Re= 0.5 – $1.0*10^6$ - domain of small and medium size UAV. At higher Reynolds numbers, increase of maximum lift of MS-airfoils comes with a gradual loss of mild stall characteristics. It is feasible to retain high lift / mild stall at reduced Reynolds numbers bellow Re= $0.5*10^6$, adjusting upper surface of MS-airfoils to formation of enlarged laminar separation bubble.
- Highly cambered, blunt MS-airfoils show increased parasite drag relative to typical NLF airfoils with moderate maximum lift. This may be tolerable in development of operational UAV, considering their specific drag build-up and clear preference for high lift.
- For MS-airfoils, the speed safety margins in development of UAV may be reconsidered, effecting the issues of high-lift loitering, take-off/landing and capability to ensure the safe flight close to stall angles of attack. Contaminated MS-airfoils retain their mild stall characteristics, allowing continuation of UAV mission in unfavorable weather conditions.

References

[1] Koss D., Steinbuch M., Shepshelovich M., "Design and experimental Evaluation of High-Lift, Mild-Stall Airfoil", *12th AIAA Applied Aerodynamics Conference*, June, 1994.

[2] Koss D., Steinbuch M. and Shepshelovich M., "Development of Two-Element NLF Airfoils for Long Endurance Flight". *35th Aerospace Sciences Meeting and Exhibit*, Reno, NV, January 6-10, 1997.

[3] Steinbuch M., Marcus B. and Shepshelovich M., "Development of UAV Wings - Subsonic Designs". *41nd Aerospace Sciences Meeting and Exhibit*, Reno, NV, 6-9 January, 2003.

[4] Shepshelovich M., "Aerodynamic Concept of IAI Long Endurance UAV". *44th Israel Annual Conference on Aerospace Sciences*, 25-26 February, 2004.

[5] McMasters J.H., Henderson M.L., "Low-Speed, Single-Element Airfoil Synthesis", Boeing Commercial Airplane Co., *MPA Symposium*, 1978.

[6] Liebeck R.H., "Subsonic Airfoil Design", Applied Computational Aerodynamics, *Progress in Astronautics and Aeronautics*, Vol. 125, 1990.

[7] Abbott I.H. and Von Doenhoff A.E., “Theory of Wing Sections”, *Dover Publications Inc*., N.Y., 1959.

[8] Althaus D. and Wortmann F.X., “Stuttgarter Profilkatalog”, *Wieweg & Sohn*, Brounschweig, 1981.

[9] Maghmer M.D. and Somers D.M., “Design and Experimental Results for a High-Altitude, Long-Endurance Airfoil”, *Aircraft*, vol. 26, No. 2, 1989.

[10] Hicks R.M. and Schairer E.T., “Effects of Upper Surface Modification on the Aerodynamic Characteristics of the NACA 63_2-215 Airfoil Section”, *NACA TM78503*, 1979.

[11] McGhee R.J. and Beasley W.D., “Wind-Tunnel Results for a Hodified 17-Percent-Thick Low-Speed Airfoil Section”, *NACA Technical Paper 1919*, 1981.

[12] Drela M., “Newton Solution of Coupled Viscous-Inviscid Multi-Element Airfoil Flow”, *AIAA 90-1470, AIAA Fluid Dynamics, Plasmodynamics and Laser Conference*, Seattle, WA, June 1990.

[13] Drela M., “A User’s Guide to MSES 2.95”, *MIT Computational Aerospace Laborator*y, September 1996.

[14] Koss D., Bauminger S., Shepshelovich M., Seifert A. and Wygnansky I., “Pilot Test of Low Reynolds Number DTE-Airfoil”, *AIAA 93-0643, 31st Aerospace Sciences Meeting and Exibit,* Reno, NV, 11-14 January, 1993.

[15] Nagel A. and Shepshelovich M., “Development of High Lift, Mild Stall Airfoils”. *44th Israel Annual Conference on Aerospace Sciences*, 25-26 February, 2004.